J. Fluid Mech. (1994), *vol.* 268, *pp.* 211–229

On coupling between the Poincaré equation and the heat equation

By KEKE ZHANG

Department of Mathematics, University of Exeter, Exeter EX4 4QJ, UK
and Isaac Newton Institute for Mathematical Sciences, Cambridge, CB3 0EZ, UK

(Received 10 September 1992 and in revised form 12 January 1994)

It has been suggested that in a rapidly rotating fluid sphere, convection would be in the form of slowly drifting columnar rolls with small azimuthal scale (Roberts 1968; Busse 1970). The results in this paper show that there are two alternative convection modes which are preferred at small Prandtl numbers. The two new convection modes are, at leading order, essentially those inertial oscillation modes of the Poincaré equation with the simplest structure along the axis of rotation and equatorial symmetry: one propagates in the eastward direction and the other propagates in the westward direction; both are trapped in the equatorial region. Buoyancy forces appear at next order to drive the oscillation against the weak effects of viscous damping. On the basis of the perturbation of solutions of the Poincaré equation, and taking into account the effects of the Ekman boundary layer, complete analytical convection solutions are obtained for the first time in rotating spherical fluid systems. The condition of an inner sphere exerts an insignificant influence on equatorially trapped convection. Full numerical analysis of the problem demonstrates a quantitative agreement between the analytical and numerical analyses.

1. Introduction

The subject of rotating fluid dynamics contains two important but traditionally separate branches: inertial oscillation and convection. Inertial oscillation usually describes the motion of an inviscid fluid in a rotating fluid container, influenced weakly by viscous dissipations that mainly occur in boundary layers. Convection in a rotating fluid container usually concerns the fluid motions driven by external forces such as thermal buoyancy, and internal viscous dissipations often play a key role in determining the basic properties of convection. Both inertial oscillation and convection in rotating spherical systems have been extensively investigated.

Inertial oscillation in rotating systems is governed by the Poincaré equation, solutions of which for a sphere, with the general implicit form in modified oblate spheroidal coordinates, have been available for a long time (Bryan 1889; Lyttleton 1953). If the fluid viscosity is completely neglected, the solutions must satisfy only the inviscid boundary condition. Most of the earlier research results concerning this problem can be found in Greenspan (1968).The convincing experimental studies by Aldridge & Toomre (1969) demonstrated the existence of inertial oscillations in rotating spherical fluid systems. Also, a variation principle was used by Aldridge (1972) for obtaining the axisymmetric solutions of the Poincaré equation in a thick spherical shell; the important application to the dynamics of the Earth's fluid core was discussed by Aldridge & Lumb (1987). In recent studies on the form of the inertial waves (Zhang

1993), it was revealed that the fluid motions described by the Poincaré equation, with a sufficiently simple structure along the axis of rotation and small azimuthal scale, must be trapped in an equatorial-waveguide tube with characteristic latitudinal half-width $(2/m)^{\frac{1}{2}}$ and radial half-width $(1/m)$, m being the azimuthal wavenumber. As a consequence, the boundary conditions at the inner spherical surface and at higher latitudes are of secondary significance.

For the problem of convection, an additional equation governing the supply of energy is required. Convection in a rotating spherical system in most cases is driven by buoyancy forces; the formulation of the problem and the earlier research results were presented in Chandrasekhar (1961). The fundamental theoretical work on convection in rapidly rotating spherical systems was carried out by Roberts (1968), Busse (1970) and Soward (1977). It was predicted that convection would be in the form of slowly drifting columnar rolls with small azimuthal scale, but the precise structure of the convection was not determined by the theories. Experimental studies by Carrigan & Busse (1983) confirmed the qualitative features predicted by the theories for the Prandtl number of the working fluid (water at room temperature, $Pr \approx 7$). Recent investigations (Zhang & Busse 1987; Zhang 1992) suggest, however, that the form of the convection pattern is dependent on the size of the Prandtl number, which is a property of the fluid. A comprehensive review of convection in rotating spherical systems can be found in, for example, Fearn, Roberts & Soward (1988) and Proctor (1994).

This paper represents an attempt to link the two traditionally separate branches of rotating spherical fluid systems – inertial oscillation and convection – and is mainly concerned with convection modes that are in addition to the slowly drifting columnar mode predicted by Busse (1970) and the spiralling mode recently studied by Zhang (1992). It is discovered in this work that, at leading order, a particular class of inertial oscillation modes described by the Poincaré equation are the preferred convection modes at small Prandtl numbers. It is at next order that buoyancy forces drive the oscillation against the weak effects of viscous dissipation in the Ekman boundary layer. Analytical convection solutions are then obtained on the basis of the perturbation of solutions of the Poincaré equation and taking into account the effects of the Ekman boundary layer. Full numerical analysis of the same problem demonstrates a quantitative agreement between the analytical and numerical solutions which are obtained at precisely the same parameters of the problem. It is also shown that the existence of an inner sphere exerts an insignificant influence on equatorially trapped convection.

The primary objectives of this paper are thus threefold: (i) to establish a link between oscillation modes of the Poincaré equation and linear convective instabilities in rotating spherical systems by an accurate numerical analysis of the full equations; (ii) to set up a linear perturbation theory on the basis of solutions of the Poincaré equation so that analytical convection solutions can be found; and (iii) to compare the results of the numerical analysis with those obtained from the perturbation theory. In the limit of $Pr\, m^{-\frac{5}{2}} \ll E$, E being the Ekman number, a complete analytical solution for convection – the critical parameters for the onset of convection, and the structure of the flow and temperature – is obtained analytically in closed form. Outside this limit, an expansion in spherical Bessel functions is used to obtain approximate solutions of the heat equation. It is then shown that a small number of terms in the expansion gives rise to an approximation with better than 1% accuracy. A reasonably satisfactory quantitative agreement between the analytical results for a full sphere and the numerical results for a thick spherical shell is reached.

2. Mathematical formulation

Consider a Boussinesq-fluid spherical shell with constant thermal diffusivity κ, thermal expansion coefficient α and kinematic viscosity ν that is rotating uniformly with a constant angular velocity Ω in the presence of its own gravitational field

$$\boldsymbol{g} = -\gamma \boldsymbol{r}, \tag{2.1}$$

where γ is a constant. A traditional heating model (Chandrasekhar 1961) is adopted, in which the basic temperature gradient,

$$\nabla T_s = -\beta \boldsymbol{r}, \tag{2.2}$$

where β is a constant, assumes a uniform distribution of heat sources. Using the thickness of the fluid shell, $d = r_o - r_i$, as the lengthscale, d^2/ν as the unit of time, and $\beta d^2 \nu/\kappa$ as the unit of temperature fluctuation of the system, the problem of convective instability, which was first formulated by Chandrasekhar (1961), is governed by the following equations:

$$\mathrm{i}\omega \boldsymbol{u} + 2\boldsymbol{k} \times \boldsymbol{u} = -\nabla P + R(1-\eta)^4 \Theta \boldsymbol{r} + \frac{E}{(1-\eta)^2} \nabla^2 \boldsymbol{u}, \tag{2.3}$$

$$\nabla \cdot \boldsymbol{u} = 0, \tag{2.4}$$

$$\left[\nabla^2 - \mathrm{i}\frac{Pr}{E}(1-\eta)^2 \omega\right] \Theta = -\boldsymbol{r} \cdot \boldsymbol{u}, \tag{2.5}$$

where $\boldsymbol{k}$ is a unit vector parallel to the axis of rotation, $\eta = r_i/r_o$, and $\boldsymbol{u}$ is the three-dimensional velocity field, (u_r, u_θ, u_ϕ), in spherical polar coordinates in the form

$$(u_r, u_\theta, u_\phi)(r, \theta, \phi, t) = (u_r, u_\theta, u_\phi)(r, \theta, \phi)\, \mathrm{e}^{\mathrm{i}\omega t}. \tag{2.6}$$

For a convenient comparison with the standard form of the Poincaré equation, the frequency ω in (2.3) and (2.5) is scaled by the rotation rate Ω. The temperature deviation from the purely conductive state, T_s, is represented by Θ, and the non-dimensional parameters – the Rayleigh number R, the Prandtl number Pr and the Ekman number E – are defined as

$$R = \frac{\alpha\beta\gamma r_o^4}{\Omega\kappa}, \quad Pr = \frac{\nu}{\kappa}, \quad E = \frac{\nu}{\Omega r_o^2}.$$

The Rayleigh number R is effectively the ratio of destabilizing forces to the Coriolis and dissipative forces, the Prandtl number Pr provides a measure of the relative importance of viscous and thermal diffusions and the Ekman number E is related to the ratio of viscous forces to the Coriolis force. In comparison with the definition of the Rayleigh number given by Chandrasekhar (1961) (see also Zhang 1992), R_{ch}, our Rayleigh number R is normalized by the Ekman number, that is $R = ER_{ch}$, to avoid large numerical values of the critical Rayleigh number in the case of small Ekman number. The velocity boundary conditions assumed in this paper are *stress-free* and impenetrable, which give

$$\frac{\partial(u_\phi/r)}{\partial r} = \frac{\partial(u_\theta/r)}{\partial r} = u_r = 0 \tag{2.7}$$

at the inner and outer bounding spherical surfaces. While the stress-free boundary conditions are appropriate for application to atmospheres, they preclude application

to the Earth's fluid core. However, we may expect that the Ekman boundary layer with the non-slip condition would make the adjustment over a short distance with little effect on the interior convection. Perfect thermally conducting boundaries impose the following conditions:

$$\Theta(r_i, \phi, \theta) = \Theta(r_o, \phi, \theta) = 0. \tag{2.8}$$

Equations (2.3)–(2.5) with boundary conditions (2.7) and (2.8) form a convective stability problem which is solved both numerically and analytically. In the numerical analysis, an inner sphere with $\eta = 0.2$ is focused on because this value is close to zero but large enough to allow our numerical solutions to converge rapidly, while the other values of η are also used to show that solutions are hardly affected by the presence of an inner core at sufficiently large wavenumbers; in the perturbation analysis a full sphere is considered by setting $\eta = 0$.

3. Numerical analysis

For the numerical analysis, a velocity field satisfying (2.4) can be written as a sum of poloidal and toroidal vectors:

$$\boldsymbol{u} = \boldsymbol{\nabla} \times \boldsymbol{\nabla} \times \boldsymbol{r} v + \boldsymbol{\nabla} \times \boldsymbol{r} w. \tag{3.1}$$

It follows that the velocity boundary condition (2.7) at the inner and outer bounding spherical surfaces becomes

$$\frac{\partial^2 v}{\partial r^2} = \frac{\partial (w/r)}{\partial r} = v = 0. \tag{3.2}$$

The poloidal and toroidal fields, v and w, and the temperature deviation, Θ, are then expanded in terms of spherical harmonics and the radial functions satisfying the boundary conditions (see Zhang & Busse 1987), for example,

$$v = \sum_{l,n} v_{lmn} \sin n\pi (r - r_i)\, Y_l^m(\theta, \phi)\, \mathrm{e}^{\mathrm{i}\omega t}, \tag{3.3}$$

where the $Y_l^m(\theta, \phi)$ are normalized such that the spherical surface integral

$$\frac{1}{4\pi} \int_S |Y_l^m(\theta, \phi)|^2 \sin\theta \, \mathrm{d}\theta \, \mathrm{d}\phi = 1.$$

The method used by Zhang & Busse (1987) for determining the onset of convection involves iterations of the determinant of a complex matrix, which becomes increasingly difficult numerically as the dimension of the complex matrix becomes large. Several other methods, including the use of the standard NAG subroutine for the complex eigenvalue problem and explicit time-integration of the equations, were considered and discarded because they are ineffective and require too much computing time. An iterative method based on the Newton–Raphson scheme is adopted which appears particularly appropriate for the problem of convective instability with large rotation rate. For a given azimuthal wavenumber, Ekman number and Prandtl number, instead of solving for only the critical parameters – the Rayleigh number R and the frequency ω – at the onset of convection, we iterate to obtain simultaneously the critical parameters R and ω and the associated convection solution. A solution vector of convection can be written in the form

$$\boldsymbol{V} = (v, w, \Theta),$$

where the coefficients of the expansions of v, w, Θ are arranged as a one-dimensional array

$$X = [X_j, j = 1, \ldots, K] = [v_1^r, v_1^i, v_2^r, v_2^i, \ldots, w_1^r, w_1^i, w_2^r, w_2^i, \ldots, \Theta_1^r, \Theta_1^i, \Theta_2^r, \Theta_2^i, \ldots,]$$

where K is a function of the truncation parameter N_t (Zhang & Busse 1987). Roughly speaking, the maximum l of spherical harmonics $Y_l^m(\theta, \phi)$ included in expansions like (3.3) is given by $m+2N_t$. We may set the real part of $v_1, v_1^r = X_1 = 1$, and the imaginary part $v_1^i = X_2 = 0$, because of the two freedoms of the linear system: amplitude and azimuthal phase. For a solution vector with dimension K, the Galerkin spectral method results in K linear real equations for given E, Pr and m,

$$f_i = f_i(R, \omega, X_j, j = 3, \ldots, K), \quad i = 1, \ldots, K.$$

Given an arbitrary initial vector X^0 and a guess for R^0 and ω^0, we can iterate this linear system in the following way:

$$R^{n+1} = R^n - \left(\frac{\partial f_1}{\partial X_j}\right)^{-1} f_j(X^n), \tag{3.4}$$

$$\omega^{n+1} = \omega^n - \left(\frac{\partial f_2}{\partial X_j}\right)^{-1} f_j(X^n), \tag{3.5}$$

$$X_i^{n+1} = X_i^n - \left(\frac{\partial f_i}{\partial X_j}\right)^{-1} f_j(X^n), \quad i = 3, \ldots, K, \tag{3.6}$$

where the superscript n denotes the nth iteration, and

$$\frac{\partial f_i}{\partial X_1} \equiv \frac{\partial f_i}{\partial R}; \frac{\partial f_i}{\partial X_2} \equiv \frac{\partial f_i}{\partial \omega}.$$

The derivatives $\partial f_i / \partial X_j$ are evaluated analytically at X^n. Typically, with an arbitrary initial X^0 and reasonable guesses for R^0 and ω^0, a convection solution converges after about four iterations; that is

$$\max\left[\frac{|R^{n+1}-R^n|}{R^{n+1}}; \frac{|\omega^{n+1}-\omega^n|}{|\omega^{n+1}|}; \frac{|X_i^{n+1}-X_i^n|}{|X_i^{n+1}|}, \quad i = 3, \ldots, K\right] \leqslant \epsilon \tag{3.7}$$

where ϵ is 10^{-6} in this paper.

4. Classification of the convection mode

We first summarize the classification of convection modes in rotating spherical systems in the parameter space of the problem suggested by our numerical analysis. Consider a rotating spherical system characterized by a fixed rotation rate and viscosity, and imagine that the thermal diffusivity, κ, is increased from a small value ($\kappa \ll \nu, Pr \gg 1$) to an asymptotically large value ($\kappa \gg \nu, Pr \ll 1$) while keeping all other parameters of the system unchanged. It is found that four different forms of convection can be observed in the following sequence:

(I) A columnar convection mode with rolls aligning with the axis of rotation and intercepting the outer spherical surface at middle latitudes; the azimuthal lengthscale of the roll is much shorter than the radial lengthscale (Busse 1970; see also Zhang 1991).

(II) A spiralling columnar convection mode in the form of eastward-spiralling drifting columnar rolls; as a consequence, the azimuthal lengthscale becomes comparable with the radial scale (Zhang 1992).
(III) An equatorially trapped Poincaré convection mode travelling in the eastward direction. In the leading order, the frequency of convection is given by

$$\omega^- = \frac{2}{l}\left(1 - \left[\frac{l^2-1}{2l-1}\right]^{\frac{1}{2}}\right), \tag{4.1}$$

and the corresponding velocity of convection can be expressed as

$$U_s = -\mathrm{i}[a_s s^{l-1} + bz^2 s^{l-3} + cs^{l-3}]\mathrm{e}^{\mathrm{i}(m\phi+\omega t)}, \tag{4.2}$$

$$U_\phi = [a_\phi s^{l-1} + bz^2 s^{l-3} + cs^{l-3}]\mathrm{e}^{\mathrm{i}(m\phi+\omega t)}, \tag{4.3}$$

$$U_z = -\mathrm{i}dzs^{l-2}\mathrm{e}^{\mathrm{i}(m\phi+\omega t)}, \tag{4.4}$$

where m is the azimuthal wavenumber, and l is an index for the solution of Poincaré modes (see Zhang 1933 for details) that is set to $l = m+2$ in this paper. Cylindrical coordinates, (s, ϕ, z), with the axis of rotation at $s = 0$, are used in (4.2)–(4.4). The coefficients are

$$a_\phi = \frac{(2l-1)(2l+l\omega-2\omega)}{8(1-l)}, \quad a_s = \frac{(2l-1)(2l+l\omega-4)}{8(1-l)},$$

$$b = \frac{(2l-1)(l-2)\omega^2}{4(\omega-2)}, \quad c = \frac{(l-2)}{(2-\omega)}, \quad d = \frac{(2l-1)\omega}{2}.$$

(IV) An equatorially trapped Poincaré mode, but travelling in the westward direction. In the leading order, the frequency of convection is

$$\omega^+ = \frac{2}{l}\left(1 + \left[\frac{l^2-1}{2l-1}\right]^{\frac{1}{2}}\right), \tag{4.5}$$

and the corresponding velocity of convection can be obtained from (4.2)–(4.4) by replacing ω^- with ω^+. The equatorially trapped convection mode III was first suggested by Zhang & Busse (1987) but without recognizing that it corresponds to the mode of the Poincaré equation. The ω^+ convection mode, which becomes the most unstable mode at even lower Prandtl numbers, was found after a pair of the equatorially trapped waves (ω^+ and ω^-) had been obtained in the Poincaré equation for this particular class (Zhang 1993).

The link between an oscillation mode of the Poincaré equation and a convection mode is established mainly based on the facts that (i) there is very little difference between the frequencies of the convection mode and the Poincaré oscillation mode, (ii) the form of the convection mode and that of the Poincaré oscillation mode are almost identical, and (iii) a good agreement between the perturbation analysis on the basis of the Poincaré mode and the full numerical analysis is reached.

While transition from mode I to mode II is gradual (Zhang 1992), the value of the Prandtl number at which the preferred convection is changed from mode II to III is dependent on the Ekman number. For example, our numerical analysis indicates the following approximate regions of the Prandtl number at $E = 10^{-4}$ occupied by each of the four forms of convection: $\infty > Pr > 1$, mode I; $1 > Pr > 0.05$, mode II; $0.05 > Pr > 0.002$, mode III; $0.002 > Pr \geqslant 0$, mode IV. A complete determination of

the different regions in the parameter space of the problem requires a theory for the columnar convection that is valid not only for small Ekman numbers but also for finite azimuthal wavenumbers, which is still not available.

It should be pointed out that there are fundamental differences between the columnar convection modes (I and II) and the Poincaré convection modes (III and IV). These may be readily seen from the equation of vorticity obtained from (2.3) in the limit $\eta = 0$:

$$2\boldsymbol{k}\cdot\nabla\boldsymbol{u} = \mathrm{i}\omega\nabla\times\boldsymbol{u} - R\nabla\Theta\times\boldsymbol{r} + E\nabla^2\nabla\times\boldsymbol{u}. \tag{4.6}$$

Note that the Proudman–Taylor condition $\boldsymbol{k}\cdot\nabla\boldsymbol{u} = 0$ cannot be satisfied because of the boundary condition: a constraint that needs to be broken in order that convection takes place (Busse 1982). In the case of the columnar convection modes (I and II), the frictional forces play a key role in breaking the constraint of rotation,

$$|2\boldsymbol{k}\cdot\nabla\boldsymbol{u}| \sim |E\nabla^2\nabla\times\boldsymbol{u}|. \tag{4.7}$$

The scale of convection rolls thus decreases rapidly with increasing rate of rotation, $m \sim E^{-\frac{1}{3}}$ (Roberts 1968). In the case of the Poincaré convection modes (III and IV), the frictional forces play a secondary role in breaking the constraint of rotation. The primary balance in (4.6) is

$$|2\boldsymbol{k}\cdot\nabla\boldsymbol{u}| \sim |\mathrm{i}\omega\nabla\times\boldsymbol{u}| \tag{4.8}$$

and, therefore, a small scale of convection cells is not necessarily required. In terms of the speed of wave propagation, the columnar convection modes (I and II) are slow and the Poincaré convection modes (III and IV) are fast.

5. Perturbation analysis

The fact that, in the present case, inertial oscillation is weakly coupled with convection, and the relevant solutions of the Poincaré equation are fairly simple, suggests an analytical perturbation approach. We can assume the following expansion:

$$\boldsymbol{u} = \boldsymbol{U} + \boldsymbol{u}_1, \quad P = P_0 + P_1, \quad \omega = \omega_0 + \omega_1,$$

where $\boldsymbol{u}_1$, P_1 and ω_1 represent small perturbations from the solutions of the Poincaré equation for the limit $E = 0$, which are denoted by $\boldsymbol{U}$, P_0 and ω_0. The requirement for the validity of the above expansion is

$$Em^2 \ll \omega_0. \tag{5.1}$$

If this condition is not satisfied, the viscous term in (4.6) would be of the same order as the other terms, which is the case for slow columnar convection (Roberts 1968), where $\omega \sim E^{\frac{1}{3}}$ and $m \sim E^{-\frac{1}{3}}$. For the Poincaré convection mode, condition (5.1) may be expressed as

$$Em^{\frac{5}{2}} \ll 1. \tag{5.2}$$

In contrast to previous analysis, the expansion is not restricted to asymptotically large wavenumber m. Substituting the expansion into (2.3)–(2.5), the zeroth order of the perturbation problem yields

$$\mathrm{i}\omega_o\,\boldsymbol{U} + 2\boldsymbol{k}\times\boldsymbol{U} + \nabla P_0 = 0, \tag{5.3}$$

$$\nabla\cdot\boldsymbol{U} = 0, \tag{5.4}$$

where $\boldsymbol{U}$ satisfies the inviscid boundary condition $U_r = 0$. Equations (5.3) and (5.4) can be combined to form the Poincaré equation for inertial oscillation (Greenspan 1968).

The solutions of the Poincaré equation for various classes and different symmetries in the form of equatorially trapped waves have recently been studied in detail by Zhang (1993). However, it should be emphasized that U *does not satisfy* the stress-free boundary condition:

$$\frac{\partial(U_\phi/r)}{\partial r} \neq 0, \frac{\partial(U_\theta/r)}{\partial r} \neq 0 \quad \text{at} \quad r = r_o.$$

The next order of the perturbation in the limit $\eta = 0$ gives rise to

$$\mathrm{i}\omega_o \boldsymbol{u}_1 + 2\boldsymbol{k} \times \boldsymbol{u}_1 + \nabla P_1 = Rr\Theta + E\nabla^2(\boldsymbol{U} + \boldsymbol{u}_b) - \mathrm{i}\omega_1 \boldsymbol{U}, \tag{5.5}$$

$$(\nabla^2 - \mathrm{i}\omega_o E^{-1} Pr)\,\Theta = -\boldsymbol{r} \cdot \boldsymbol{U}, \tag{5.6}$$

$$\nabla \cdot \boldsymbol{u}_1 = 0, \tag{5.7}$$

where $\boldsymbol{u}_1 = \boldsymbol{u}_i + \boldsymbol{u}_b$, $\boldsymbol{u}_i$ is the perturbation of the interior flow and $\boldsymbol{u}_b$ is the boundary flow associated with the Ekman layer, which is non-zero only in the vicinity of the outer spherical boundary surface. While $\boldsymbol{u}_i$ is a small perturbation relative to the zeroth-order velocity $\boldsymbol{U}$, the boundary flow $\boldsymbol{u}_b$ has to be large enough so that $(\boldsymbol{u}_b + \boldsymbol{U})$ satisfies the stress-free boundary condition. It will be shown that the Ekman boundary layer plays an essential role in the convective instability problem associated with the Poincaré mode, but the precise structure of the boundary-layer flow is not needed for the linear instability problem with the stress-free boundary condition.

Denote the complex conjugate of $\boldsymbol{U}$ by $\boldsymbol{U}^*$, which also satisfies $\nabla \cdot \boldsymbol{U}^* = 0$ and the boundary condition $U_r^* = 0$, multiply (5.5) by $\boldsymbol{U}^*$ and integrate over the volume of the sphere. The left-hand side of (5.5) then becomes

$$\int_v \boldsymbol{U}^* \cdot (\mathrm{i}\omega_o \boldsymbol{u}_1 + 2\boldsymbol{k} \times \boldsymbol{u}_1 + \nabla P_1)\,\mathrm{d}V = \int_v \boldsymbol{u}_1 \cdot (\mathrm{i}\omega_o \boldsymbol{U}^* - 2\boldsymbol{k} \times \boldsymbol{U}^*)\,\mathrm{d}V, \tag{5.8}$$

where we use $$\int_v \boldsymbol{U}^* \cdot \nabla P_1\,\mathrm{d}V = \int_s P_1 U_r^*\,\mathrm{d}S = 0$$

and $\int_s \mathrm{d}S$ represents the surface integral over the outer spherical surface. But the complex-conjugate velocity $\boldsymbol{U}^*$ satisfies the following equation:

$$\mathrm{i}\omega_o \boldsymbol{U}^* - 2\boldsymbol{k} \times \boldsymbol{U}^* = \nabla P_o^*. \tag{5.9}$$

It is then readily shown that the integral given by (5.8) vanishes. It follows that the solvability conditions, where the real part corresponds to the critical Rayleigh number for the onset of convection and the imaginary part gives rise to the correction for frequency, can be expressed as

$$\mathrm{Re}\left[R\int_v \boldsymbol{U}^* \cdot r\Theta\,\mathrm{d}V\right] = -\mathrm{Re}\left[E\int_v \boldsymbol{U}^* \cdot \nabla^2(\boldsymbol{U} + \boldsymbol{u}_b)\,\mathrm{d}V\right], \tag{5.10}$$

$$\mathrm{Im}\left[R\int_v \boldsymbol{U}^* \cdot r\Theta\,\mathrm{d}V\right] = -\mathrm{Im}\left[E\int_v \boldsymbol{U}^* \cdot \nabla^2(\boldsymbol{U} + \boldsymbol{u}_b)\,\mathrm{d}V\right] + \omega_1 \int_v |\boldsymbol{U}|^2\,\mathrm{d}V. \tag{5.11}$$

Note that $\boldsymbol{U}$ is a function of ω^+ or ω^- defined by (4.1) and (4.5). The physically observed Poincaré convection mode is then related to the most unstable mode of convective instability,

$$R_c(m, \omega^+, \omega^-, Pr, E) = \mathrm{Min}.$$

That is, for given values of E and Pr, the Rayleigh numbers are calculated with different wavenumbers m and different modes of the Poincaré equation to obtain the lowest Rayleigh number R_c. Convection in the form of inertial oscillation, described by the Poincaré equation and weakly modified by the effects of viscosity, will then be sustained when the Rayleigh number R is slightly greater than R_c, assuming that the corresponding bifurcation is supercritical; the system is, however, in a motionless conducting state when $R < R_c$. A complete solution of convection in a spherical fluid system with given E and Pr may be represented in the leading order by

$$(R_c, m, U, \omega_0 + \omega_1, \Theta),$$

where U and ω_0 are the solutions of the Poincaré equation given by (4.1)–(4.5), and Rc, m, ω_1 can be determined when temperature Θ, the solution of (5.6), is obtained. In the limit of $Pr\, m^{-\frac{5}{2}} \ll E$, the whole problem can be fully solved analytically in closed form; otherwise temperature Θ in (5.6) has to be determined approximately by an analytical expression.

5.1. *Analysis with the limit* $Pr\, m^{-\frac{5}{2}} \ll E$

In the limit $Pr\, m^{-\frac{5}{2}} \ll E$, the second term in the left-hand side of (5.6) can be neglected and temperature Θ is then decomposed into two parts:

$$\Theta = \Theta_0(r, \theta, \phi, t) + T(r, \theta, \phi, t), \tag{5.12}$$

where T satisfies $\nabla^2 T = 0$, but with an inhomogeneous boundary condition, and Θ_0 satisfies an inhomogeneous differential equation, but with a homogeneous boundary condition. Substituting the decomposition into (5.6), we obtain an equation for Θ_0:

$$\nabla^2 \Theta_0 = -\mathrm{i}[a_s s^{m+2} + (d+b) s^m z^2 + c s^m] \, \mathrm{e}^{\mathrm{i}(m\phi + \omega_0 t)} \tag{5.13}$$

which permits solutions of the form

$$\Theta_0 = \mathrm{i}(A s^{m+4} + B s^{m+2} + C z^2 s^{m+2}) \, \mathrm{e}^{\mathrm{i}(m\phi + \omega_0 t)}. \tag{5.14}$$

The constants A, B, C can be determined by comparing both sides of (5.6) after substitution,

$$A = \frac{a_s}{8l} - \frac{(d+b)}{16l(l-1)}, \quad B = \frac{c}{4(l-1)}, \quad C = \frac{d+b}{4(l-1)},$$

where, as a reminder, $l = m+2$. The boundary condition for T is then given by

$$T(1, \theta, \phi, t) = -\mathrm{i}(A \sin^{l+2}\theta + B \sin^{l}\theta + \tfrac{1}{4} C \sin^2(2\theta) \sin^{l-2}\theta) \, \mathrm{e}^{\mathrm{i}(m\phi + \omega_0 t)}. \tag{5.15}$$

The exact solution of $\nabla^2 T = 0$ satisfying the boundary condition (5.15) has the form

$$T(r, \theta, \phi, t) = -\mathrm{i} \sin^m \theta \sum_{k=m}^{m+4} T_k r^k \frac{\partial^m P_k(\cos\theta)}{\partial(\cos\theta)^m} \mathrm{e}^{\mathrm{i}(m\phi + \omega_0 t)}, \tag{5.16}$$

where T_k are coefficients and $P_k(\cos\theta)$ is the Legendre function. The equatorial symmetry

$$T(r, \theta, \phi) = T(r, \pi - \theta, \phi)$$

leads to $$T_k = 0 \quad \text{if} \quad k = m+1, m+3.$$

Some manipulations then give

$$T(s, \phi, z, t) = -\mathrm{i}[B_1 s^m + B_2 s^m z^2 + B_3 s^{m+2} + B_4 s^m z^4 + B_5 s^{m+2} z^2 + B_6 s^{m+4}] \, \mathrm{e}^{\mathrm{i}(m\phi + \omega_0 t)}, \tag{5.17}$$

where the coefficients are a function of A, B, C and m:

$$B_1 = (A+B)+\frac{C-2A-B}{2m+3}+\frac{3A-3C}{(2m+3)(2m+5)},$$

$$B_2 = \frac{2m+2}{(2m+3)(2m+7)}[2m(C-2A-B)+C-8A-7B],$$

$$B_3 = \frac{-1}{(2m+3)(2m+7)}[2m(C-2A-B)+C-8A-7B],$$

$$B_4 = \frac{[(2m+5)(2m+1)+3]}{(2m+5)(2m+7)}(A-C),$$

$$B_5 = \frac{(-12m-24)}{(2m+5)(2m+7)}(A-C),$$

$$B_6 = \frac{3}{(2m+5)(2m+7)}(A-C).$$

The exact solution of (5.6) in complex form is

$$\Theta = -\mathrm{i}[B_1 s^m + B_2 s^m z^2 + (B_3-B)\, s^{m+2} + B_4 s^m z^4 + (B_5-C)\, s^{m+2} z^2 + (B_6-A)\, s^{m+4}]\, \mathrm{e}^{\mathrm{i}(m\phi+\omega_0 t)}. \quad (5.18)$$

5.2. *The importance of the Ekman layer*

If the effects of the Ekman boundary layer are neglected in the perturbation analysis, the stability analysis is then connected with the evaluation of three complex integrals in (5.10) and (5.11) resulting from the solvability condition. It is straightforward to show that the integral

$$H_\Theta = \int_v U^* \cdot r\Theta \, \mathrm{d}V = \int_v U \cdot r\Theta^* \, \mathrm{d}V. \quad (5.19)$$

From (5.6) and Θ given by (5.18), it can be shown in the limit $Pr\, m^{-\frac{5}{2}} \ll E$ that

$$H_\Theta = \int_v U^* \cdot r\Theta \, \mathrm{d}V = \int_v |\nabla\Theta|^2 \, \mathrm{d}V$$

$$= E_6 I_{l+1,0} + E_4 I_{l-1,2} + E_3 I_{l,0} + E_5 I_{l,1} + E_2 I_{l-1,1} + E_1 I_{l-1,0} + E_7 I_{l-2,1} + E_8 I_{l-2,2} + E_9 I_{l-2,0} + E_{10} I_{l-2,3},$$

where $I_{n,j}$ is defined as $$I_{n,j} = \frac{2^{n+2}\pi n!(2j-1)!!}{(2n+2j+3)!!},$$

and the coefficients are

$$E_1 = a_s B_1 + c(B_3-B), \qquad E_2 = a_s B_2 + (d+b)(B_3-B) + (B_5-C)\, c,$$

$$E_3 = a_s(B_3-B) + c(B_6-A), \qquad E_4 = a_s B_4 + (d+b)(B_5-C),$$

$$E_5 = a_s(B_5-C) + (d+b)(B_6-A), \qquad E_6 = a_s(B_6-A),$$

$$E_7 = (d+b)\, B_1 + cB_2, \qquad E_8 = cB_4 + (d+b)\, B_2,$$

$$E_9 = B_1 c, \qquad E_{10} = B_4(d+b).$$

One unexpected result, however, is the integral associated with the term for internal viscous dissipations for the solvability conditions (5.10) and (5.11):

$$H_v = \int_v \boldsymbol{U}^* \cdot \nabla^2 \boldsymbol{U} \, \mathrm{d}V = -\frac{4}{\omega^2} \int_v \boldsymbol{U}^* \cdot (\boldsymbol{k} \cdot \nabla)^2 \boldsymbol{U} \, \mathrm{d}V$$
$$= F_m[(a_s + a_\phi) m + b + (2m+3) c],$$

where F_m is a function of wavenumber m. By using the expressions for the coefficients a_s, a_ϕ, b, c in §4 for either the ω^+ or ω^- modes, we found that this integral is identically zero. In this connection, it is worth mentioning that

$$\int_v \boldsymbol{U}_m^*(\omega^+) \cdot \boldsymbol{U}_k(\omega^-) \, \mathrm{d}V = 0 \quad \text{if} \quad m = k \tag{5.20}$$

as proved by Greenspan (1968). Here we found another interesting mathematical property of the solutions of the Poincaré equation: the velocity $\boldsymbol{U}^*$ for the class of the simplest axial structure with equatorial symmetry ((4.1)–(4.5)) is orthogonal to $\nabla^2 \boldsymbol{U}$:

$$\int_v \boldsymbol{U}_m^*(\omega^+) \cdot \nabla^2 \boldsymbol{U}_k(\omega^+) \, \mathrm{d}V = 0, \quad \int_v \boldsymbol{U}_m^*(\omega^-) \cdot \nabla^2 \boldsymbol{U}_k(\omega^-) \, \mathrm{d}V = 0 \quad \text{if} \quad m = k \tag{5.21}$$

for any non-zero azimuthal wavenumber m. Though the mathematical implication of (5.21) is still not clear, physically it implies that convection in this case is driven by the boundary stresses resulting from the inviscid boundary condition which does not satisfy the condition of the stress-free boundary. The Ekman boundary layers are therefore of essential importance in determining the stability properties of the problem even when the stress-free boundary conditions are assumed.

5.3. *Analysis with the Ekman layer*

In contrast to the analysis of Ekman boundary layers with an established flow (Greenspan 1969), the Ekman layers in the problem of rotating convection are formed at the same time as any motion takes place. In general, it is difficult to solve the exact structure of the boundary layer in convective rotating spherical systems. Fortunately, it is found that specification of the exact structure of the boundary layers can be avoided, in the leading order, by taking the boundary condition into account in a surface integral. In other words, with regard to the onset of convection with the stress-free boundary condition (2.7), the effects of viscosity in the Ekman boundary layer can be included to the extent that is possible without involving a detailed boundary-layer theory. The boundary flow $\boldsymbol{u}$ (here the subscript b for $\boldsymbol{u}$ is dropped) satisfies the following condition:

$$\frac{\partial(u_\theta/r)}{\partial r} = -\frac{\partial(U_\theta/r)}{\partial r}, \quad \frac{\partial(u_\theta/r)}{\partial r} = -\frac{\partial(U_\phi/r)}{\partial r} \tag{5.22}$$

on the outer spherical surface. The real part of the solvability condition (5.10) in the limit $Pr\, m^{-\frac{5}{2}} \ll E$ becomes

$$-R/E \int_v |\nabla \Theta|^2 \, \mathrm{d}V = \int_v \boldsymbol{U}^* \cdot \nabla^2 (\boldsymbol{U} + \boldsymbol{u}_b) \, \mathrm{d}V, \tag{5.23}$$

the right-hand side of which in the leading order is

$$H_b = \int_s 2|\,\boldsymbol{U}|^2 \, \mathrm{d}S - \int_v |\nabla \times \boldsymbol{U}|^2 \, \mathrm{d}V + \int_s \left[U_\phi^* \frac{\partial(U_\phi + (u)_\phi)/r}{\partial r} + U_\theta^* \frac{\partial(U_\theta + (u)_\theta)/r}{\partial r} \right] \mathrm{d}S. \tag{5.24}$$

Using the stress-free boundary condition, the last term involving the integral over the outer spherical surface vanishes. In deriving the above integral, we have used the fact that there are two different scales: the larger one is the radial half-width of the equatorial waveguide tube, $L = 1/m$, and the smaller one is the thickness of the Ekman boundary layer $E^{\frac{1}{2}}$. For the Poincaré convection modes, the radial half-width of the equatorial waveguide tube always satisfies $L \gg E^{\frac{1}{2}}$, a result of the condition $Em^{\frac{5}{2}} \ll 1$ for the validity of the perturbation expansion. The expression for the integral H_b in (5.24) can be further simplified by using the orthogonal condition between $\boldsymbol{U}^*$ and $\nabla^2 \boldsymbol{U}$:

$$H_b = \int_s 2|U|^2 \,\mathrm{d}S - \int_v |\nabla \times \boldsymbol{U}|^2 \,\mathrm{d}V = \int_s \left[U_\phi^* \frac{\partial (U_\phi/r)}{\partial r} + U_\theta^* \frac{\partial (U_\theta/r)}{\partial r} \right] \mathrm{d}S, \tag{5.25}$$

where only one surface integral is involved for H_b. The corresponding explicit formula for (5.25) is

$$\begin{aligned} H_b = {} & [a_\phi^2 (l-2)] J_{l-1,0} + [(2l-4)\, a_\phi b + (2l-6)\, c(a_s - d)] J_{l-2,1} \\ & + [(2l-6)\, a_\phi c] J_{l-2,0} + [(2l-6)\, bc + (l-4)\, c^2] J_{l-3,1} \\ & + [(l-2)\, b^2 + (2l-6)\, bc] J_{l-3,2} + [(l-4)\, c^2] J_{l-3,0} \\ & + [(l-2)(a_s - d)^2] J_{l-1,1} + [(2l-4)\, b(a_s - d)] J_{l-2,2} + [(l-2)\, b^2] J_{l-3,3}, \end{aligned}$$

where $J_{n,j}$ is defined as

$$J_{n,j} = \frac{2^{n+2} \pi n! (2j-1)!!}{(2n+2j+1)!!}.$$

The Rayleigh number R in (5.10) may then be expressed as

$$R = -E \int_s \left[U_\phi^* \frac{\partial (U_\phi/r)}{\partial r} + U_\theta^* \frac{\partial (U_\theta/r)}{\partial r} \right] \mathrm{d}S \Big/ \int_v |\nabla \Theta|^2 \,\mathrm{d}V = -E H_b / H_\Theta, \tag{5.26}$$

where both H_Θ and H_b are analytical functions of the azimuthal wavenumber m. Furthermore, H_Θ and H_b are pure real numbers, equation (5.11) indicating that

$$\omega_1 \int_v |\,U|^2 \,\mathrm{d}V = 0. \tag{5.27}$$

The complete convection solution in the leading order in the limit $Pr\, m^{-\frac{5}{2}} \ll E$ is thus represented by R_c by minimizing R in (5.26) over different modes and wavenumbers with the relevant $\boldsymbol{U}$ and ω in §4 and with Θ given by (5.18). The analytical results agree satisfactorily with the full numerical analysis and will be discussed in §6.

5.4. *Analysis without the limit* $Pr\, m^{-\frac{5}{2}} \ll E$

Relaxing the condition $Pr\, m^{-\frac{5}{2}} \ll E$ has two consequences. First, the effects of the Prandtl number are to cause a shift of the azimuthal phases between Θ and U_r, and as a result, a closed form of solutions for the heat equation (5.6) cannot be obtained. Secondly, a non-zero correction ω_1 to the frequency of inertial waves is expected because H_Θ becomes complex. We first solve (5.6), with which the relevant integrals in (5.10) and (5.11) for the critical Rayleigh number of convective instability can be evaluated, and then discuss the frequency modification. In order to study the dependence of the character of the system on the Prandtl number, such as the switch from the ω^+ convection mode to the ω^- mode, we choose to expand the total temperature Θ in spherical Bessel functions

$$\Theta = \sum_{l,n}^{N} \Theta_{lmn}\, Y_l^m(\theta, \phi) j_l(B_{ln} r)\, \mathrm{e}^{\mathrm{i}\omega_0 t}, \tag{5.28}$$

where $l = m, m+2$ (see the discussion below) and $n = 1, 2, \ldots, N$, N being a truncation parameter; Θ_{lmn} is a complex coefficient and B_{ln} is chosen such that

$$j_l(B_{ln}) = 0, n = 1, 2, \ldots, N.$$

$Y_l^m(\theta, \phi)$ is normalized in the same way as discussed in §3. Substituting the above expression into the heat equation, multiplying it by $[Y_l^m(\theta, \phi)]^* j_l(B_{ln} r)$, and integrating over the sphere gives

$$\Theta_{lmn} = \frac{-\mathrm{i}(B_{ln}^2 - \mathrm{i}Pr\, E^{-1}\omega_0)}{j_{l+1}^2(B_{ln})(Pr^2 E^{-2}\omega_0^2 + B_{ln}^4)\, B_{ln}^{m+5}}[a_s Z_{ln}^1 + (d+b) Z_{ln}^2 + cB_{ln}^2 Z_{ln}^3], \quad (5.29)$$

where

$$Z_{ln}^1 = \int_0^{B_{ln}} y^{m+4} j_l(y)\, \mathrm{d}y \int_{-1}^{1} (1-x^2)^{(m+2)/2} P_l^m(x)\, \mathrm{d}x,$$

$$Z_{ln}^2 = \int_0^{B_{ln}} y^{m+4} j_l(y)\, \mathrm{d}y \int_{-1}^{1} x^2 (1-x^2)^{m/2} P_l^m(x)\, \mathrm{d}x,$$

$$Z_{ln}^3 = \int_0^{B_{ln}} y^{m+2} j_l(y)\, \mathrm{d}y \int_{-1}^{1} (1-x^2)^{m/2} P_l^m(x)\, \mathrm{d}x.$$

Explicit analytical expressions can be found for all the above integrals. It is essential to observe that the integral involving the associated Legendre function $P_l^m(x)$ in Z_{ln}^3 has the following properties:

$$\int_{-1}^{1} (1-x^2)^{m/2} P_l^m(x)\, \mathrm{d}x = 0 \quad \text{if} \quad l \neq m \quad (5.30)$$

and

$$\int_{-1}^{1} (1-x^2)^{m/2} P_l^m(x)\, \mathrm{d}x = \frac{2^{m+1} m!}{[(2m+1)(2m)!]^{\frac{1}{2}}}, \quad \text{if} \quad l = m. \quad (5.31)$$

In addition, with the recurrence relation the other two integrals with $P_l^m(x)$ in Z_{ln}^1 and Z_{ln}^2 can be expressed in terms of the following integrals:

$$\int_{-1}^{1} (1-x^2)^{m/2} P_{l-2}^m(x)\, \mathrm{d}x; \quad \int_{-1}^{1} (1-x^2)^{m/2} P_l^m(x)\, \mathrm{d}x; \quad \int_{-1}^{1} (1-x^2)^{m/2} P_{l+2}^m(x)\, \mathrm{d}x.$$

The last integral is zero because $l \geqslant m$ and the first one is non-zero only if $l = m+2$. As a consequence, there are only the two relevant integrals related to the Bessel function $j_l(y)$ which can be also expressed analytically,

$$\int_0^{B_{ln}} y^{m+2} j_m(y)\, \mathrm{d}y = B_{ln}^{m+2} j_{m+1}(B_{ln}),$$

$$\int_0^{B_{ln}} y^{m+4} j_m(y)\, \mathrm{d}y = B_{ln}^{m+3}[B_{ln} j_{m+1}(B_{ln}) - 2j_{m+2}(B_{ln})].$$

Each coefficient Θ_{lmn} of expansion (5.28) is therefore an explicit analytical function of E, Pr and m. It follows that the analytical expression for the Rayleigh number R in (5.10) is

$$\frac{E}{R} = \frac{-1}{H_b} \sum_{l,n}^{N} \frac{[a_s Z_{ln}^1 + (d+b) Z_{ln}^2 + cB_{ln}^2 Z_{ln}^3]^2}{B_{ln}^{2m+8} j_{l+1}^2(B_{ln})[Pr^2 E^{-2}\omega_0^2 + B_{ln}^4]}, \quad (5.32)$$

where H_b is given by (5.25), and $l = m$, $m+2$ and $n = 1, 2, \ldots, N$. Every term in (5.32) is evaluated analytically and the size of N is chosen in accordance with the desired

accuracy. The analytical expression for the correction of the oscillation frequency is given by

$$\omega_1 = \sum_{l,n}^{N} \frac{-RPr\,E^{-1}\omega_0}{j_{l+1}^2(B_{ln})[Pr^2E^{-2}\omega_0^2 + B_{ln}^4]\,B_{ln}^{2m+10}} [a_s Z_{ln}^1 + (d+b) Z_{ln}^2 + cB_{ln}^2 Z_{ln}^3]^2 \Big/ \int_v |U|^2 \,\mathrm{d}V. \tag{5.33}$$

We observe that the frequency of the convection may be expressed as

$$\omega = \omega_0(1-h), \tag{5.34}$$

where h is a small positive constant: the effect of the Prandtl number is always to reduce the speed of the travelling wave.

6. Comparison: numerical versus analytical

Three areas of comparison are focused on. First, the critical parameters for the onset of convection, such as the Rayleigh number and oscillation frequency, are examined for several typical cases. At the same time, the accuracies of the numerical analysis and the approximation by (5.32) are discussed. Secondly, the detailed patterns of convection, the velocity and temperature fields, are compared for the numerical solution and the analytical solution at exactly the same parameters. Finally, the dependence of convection on the physical parameters, in particular the Prandtl number, is studied.

Convergence and accuracy are of importance, in particular, for comparison of the results obtained with completely different approaches. We observe from table 1 that the numerical solutions are well converged and the accuracy of our numerical analysis is better than 1%. It is also fortunate that the exact value for R given by (5.32) exists in the limit $Pr = 0$ (equation (5.26)), so that the accuracy of approximation with finite N in (5.32) can be checked with the exact Rayleigh number R given by (5.26). This is shown in table 2 in which the exact values of the critical Rayleigh number and the approximate values at different truncation levels can be compared. It indicates a fast convergence, and only three radial Bessel functions in the expansion (5.28) are needed to produce a better than 1% accuracy of approximation.

Also displayed in table 1 are the critical parameters for different wavenumbers, both numerical and analytical, for the onset of convection in several typical cases. The case of $Pr = 0$ represents the limit $Pr\,m^{-\frac{5}{2}} \ll E$ where the second term in (5.6) is neglected. For $E = 10^{-5}$ and $Pr = 0.02$, the numerical analysis for a thick spherical shell with $\eta = 0.2$ gives rise to the most unstable mode, characterized by the azimuthal wavenumber $m = 7$, the critical Rayleigh number $R_c = 24.41$ and frequency $\omega = -0.2536$. The perturbation analysis on the basis of the Poincaré modes not only closely predicts the critical Rayleigh number and frequency for a spherical shell, but also gives the same azimuthal wavenumber for the most unstable mode. The minimization of R given by (5.32) shows exactly the same wavenumber $m = 7$ for the most unstable mode (see also figure 4*a*) with $R_c = 25.68$ and $\omega = -0.2548$, where the correction of frequency by (5.33) has been taken into account. Much larger Rayleigh numbers, suggested by both the numerical and analytical results, are required in this case to excite either the columnar convection modes or the ω^+ Poincaré mode (mode IV). However, the ω^+ Poincaré mode is always preferred when $Pr\,m^{-\frac{5}{2}} \ll E$ is satisfied, again suggested by both the numerical and analytical analysis. An example for $E = 10^{-4}$ is also shown in table 2, where both the ω^+ and ω^- convection modes are presented for the case $Pr = 0$. The correction for the inertial oscillation, ω_1 is zero since the radial flow U_r that carries

	E	Pr	N_t	m	R	ω
numerical	10^{-4}	0	14	2	1.653	1.2316
	10^{-4}	0	16	2	1.660	1.2316
	10^{-4}	0	18	2	1.664	1.2316
analytical	10^{-4}	0	—	2	1.260	1.2319
numerical	10^{-4}	0	14	2	1.942	−0.2305
	10^{-4}	0	16	2	1.955	−0.2305
	10^{-4}	0	18	2	1.962	−0.2305
analytical	10^{-4}	0	—	2	1.646	−0.2319
numerical	10^{-5}	0.02	14	7	22.55	−0.2538
	10^{-5}	0.02	16	7	23.00	−0.2537
	10^{-5}	0.02	20	7	23.63	−0.2537
	10^{-5}	0.02	22	7	23.85	−0.2537
	10^{-5}	0.02	24	7	24.04	−0.2537
	10^{-5}	0.02	28	7	24.31	−0.2537
	10^{-5}	0.02	30	7	24.41	−0.2537
	10^{-5}	0.02	24	7	24.39*	−0.2535*
	10^{-5}	0.02	28	7	24.58*	−0.2535*
analytical	10^{-5}	0.02	—	7	25.68	−0.2548

TABLE 1. Examples of the convergence behaviour of full numerical solutions for $\eta = 0.2$ or $\eta = 0.35$, marked with an asterisk. The corresponding results from perturbation analysis are also presented for comparison

	Approximate			
Exact	$N = 2$	$N = 3$	$N = 4$	$N = 6$
$R_c = 1.2595$, ω^+	$R_c = 1.2629$	1.2601	1.2597	1.2596
$R_c = 1.6462$, ω^-	$R_c = 1.6507$	1.6470	1.6464	1.6462

TABLE 2. A comparison between the exact values of R_c and those obtained by approximation at $E = 10^{-4}$, $Pr = 0$ for $m = 2$, where $\omega^+ = 1.2319$, $\omega = -0.2319$

away heat and the temperature Θ have the same phase. The numerical analysis indicates that large-scale convection with $m = 2$ is preferred and that the Rayleigh number increases with increasing azimuthal wavenumber; the analytical formula given by (5.26) shows the same behaviour, but with $R(m = 2)$ slightly larger than $R(m = 1)$. Even though the effects due to the presence of the inner core cannot be completely neglected owing to large scale motions, the numerical and analytical results are still in good quantitative agreement.

Convection patterns at $E = 10^{-5}$, $m = 7$, $\eta = 0.2$ and $Pr = 0.02$ are illustrated in figure 1, where the numerical results are shown on the left-hand side of the figure and the analytical results are on the right-hand side. A dashed circle for the analytical solution indicates the position of the inner sphere which is only included in the numerical analysis. A frame moving with the phase speed of azimuthally travelling waves is used to illustrate the stationary pattern. It is worth mentioning that the phases of solution are arbitrary because of the homogeneous boundary condition: if $\boldsymbol{u}(\phi)$ is a solution, $\boldsymbol{u}(\phi + \phi_0)$ is also a solution, ϕ_0 being a constant. There is very little noticeable difference between the patterns of convection obtained from the numerical and analytical methods. Convective motions are trapped in the equatorial-waveguide tube with characteristic latitudinal half-width $(2/m)^{\frac{1}{2}}$ and radial half-width $(1/m)$. As a consequence, very little influence can be exerted on this type of convection by the

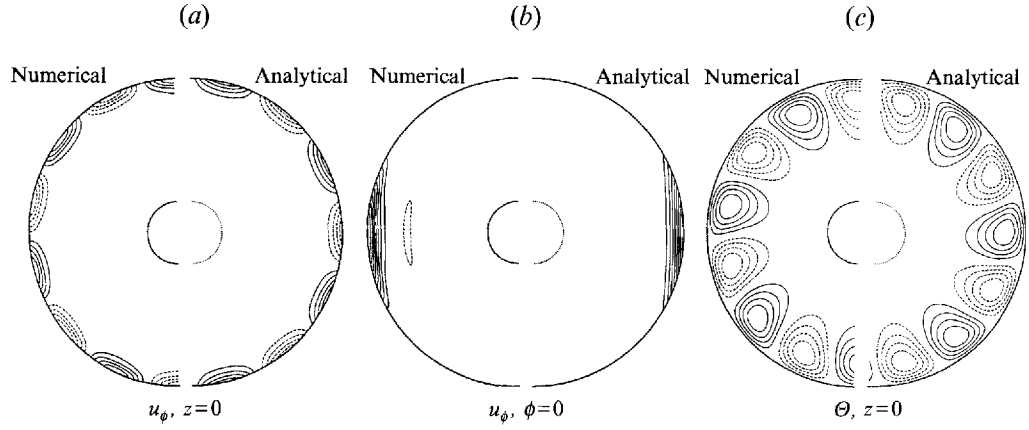

FIGURE 1. (*a*) Contours of u_ϕ at the equatorial plane, (*b*) contours of u_ϕ in a meridional plane and (*c*) contours of Θ at the equatorial plane for $E = 10^{-5}$, $Pr = 0.02$ and $m = 7$. The numerical results are on the left-hand side and the analytical results are on the right-hand side. The critical parameters are $R_c = 25.68$ and $\omega = -0.2548$ for the analytical solution, and $R_c = 24.41$ and $\omega = -0.2536$ for the numerical solution.

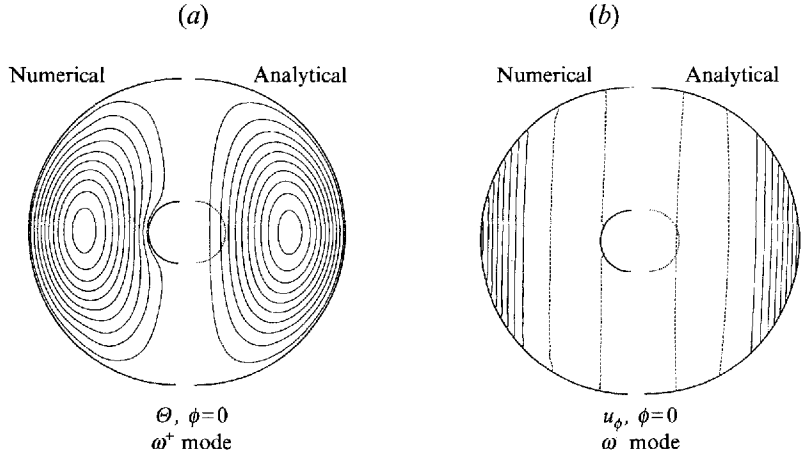

FIGURE 2. (*a*) Contours of Θ in a meridional plane for the ω^+ convection mode and (*b*) contours of u_ϕ for the ω^- convection mode at $E = 10^{-4}$, $Pr = 0$ (see table 1 for details).

presence of a small inner sphere. A solution with $E = 10^{-5}$, $m = 7$, $\eta = 0.35$ and $Pr = 0.02$ is included in table 1 to demonstrate the weak effects of the inner core. While the case with $\eta = 0.2$ gives rise to $R_c = 24.41$ and $\omega = -0.2537$, a larger inner core with $\eta = 0.35$ gives $R_c = 24.58$ and $\omega = -0.2535$.

This is, of course, not true if a large-scale convection mode is preferred. The most unstable mode with the small Prandtl numbers ($Pr\, m^{-\frac{5}{2}} \ll E$) is characterized by a large scale; the preferred modes always correspond to the ω^+ Poincaré mode, which propagates in the westward direction. An example at $E = 10^{-4}$ for both the ω^+ and ω^- convection modes is presented in figure 2. In order to satisfy the boundary condition at the inner spherical surface, there are clearly noticeable differences between the numerical solution for a spherical shell and the analytical solution for a sphere. This is illustrated in figure 2(*a*) (depicting the temperature field in a meridional plane) by comparing the numerical result on the left-hand side to the analytical solution on the right-hand side, where the temperature of the numerical solution in the vicinity of the

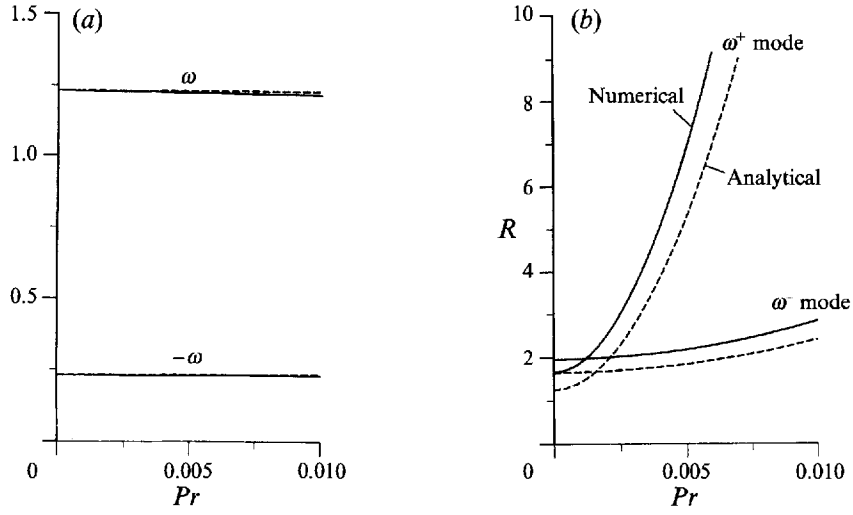

FIGURE 3. Instability curves at $E = 10^{-4}$ shown for the numerical results (solid lines) and the analytical results (dashed lines). (*a*) The oscillation frequency and (*b*) the Rayleigh number are plotted against the Prandtl number.

inner sphere has to be changed to satisfy the boundary condition. The agreement between the analytical and numerical analysis, however, is still quite satisfactory for the global-scale convection, owing largely to the rapid decay of the convection from the outer spherical surface as clearly shown in figure 2(*b*).

On the basis of (4.1)–(4.5), (5.26) and (5.32)–(5.33), the complete convection solutions of the Poincaré modes can be obtained for any values of the parameters of the problem, while it becomes increasingly difficult to obtain an accurate numerical solution for $E \leqslant 10^{-5}$. Figure 3 shows the dependence of the critical parameters on the Prandtl number at $E = 10^{-4}$ for both the numerical and analytical results with the azimuthal wavenumber $m = 2$. An excellent agreement between the perturbation and numerical results is found in the frequency curves in figure 3(*a*); the Rayleigh number curves show the same tendency but with about 15% discrepancy. The discrepancy for this large-scale mode is mainly caused by the difference between the spherical shell of the numerical results and the full sphere of the analytical results. For the localized solutions of $m = 7$, this effect is much smaller and the discrepancy is therefore much smaller. Both analyses, however, suggest the same dependence: the ω^+ mode of the large scale becomes the preferred mode with sufficiently small Prandtl numbers (see also table 1).

Instability curves resulting from (5.32) are shown in figure 4(*a*, *b*) for $E = 10^{-5}$ and 10^{-6} for different values of the Prandtl numbers. For all these Prandtl numbers, the ω^- convection modes are always preferred. An example for the ω^+ convection mode at $Pr = 0.01$ is also shown in figure 4(*a*) on the dashed curve. A particular example with $E = 10^{-5}$ and $Pr = 0.02$, which is studied in detail, has already been discussed and shown in table 1. According to both the numerical and analytical analyses, the azimuthal wavenumber for the most unstable mode is increased with increasing Prandtl number, even though the friction force does not enter the primary force balance in (4.6). Finally, it is of importance to note that in the perturbation theory presented in this paper an asymptotically large wavenumber is not required, in contrast to the previous perturbation theories of columnar modes. Moreover, the wavenumbers for the most unstable Poincaré convection modes are not always asymptotically large in a rapidly rotating fluid sphere.

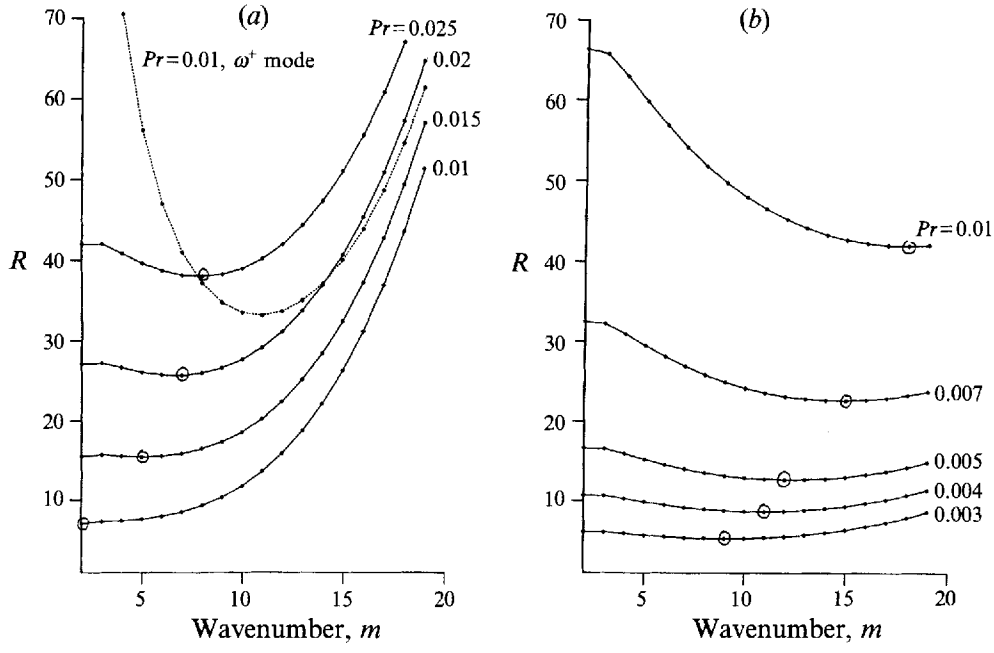

FIGURE 4. Instability curves (*a*) for $E = 10^{-5}$ and (*b*) for $E = 10^{-6}$ shown for different Prandtl numbers. The circle indicates the most unstable mode.

7. Concluding remarks

The most significant finding reported in this paper is the discovery of the link between convective instability and inertial oscillation in rotating spherical fluid systems, which has important mutual implications for both problems. On the one hand, relatively simple solutions of the Poincaré equation shed light on rotating spherical convection: this not only enables us to obtain analytical solutions of the relevant convection, but also further studies of the weakly nonlinear convection become feasible because of the availability of simple linear solutions. On the other hand, thermal instability provides a mechanism by which particular inertial oscillation modes can be excited and sustained, and provides a way to select an inertial mode by the mechanism of convective instability.

We have only investigated convection with stress-free boundary conditions, which are unrealistic when applied to many real systems such as the Earth's liquid core. The main feature of the equatorially trapped convection is that its velocity amplitude peaks at the outer spherical boundary. However, the velocity of convection with the rigid boundary conditions must completely vanish on the outer spherical boundary. Whether or not the non-slip boundary condition has significant influences on the form of convection described in this paper remains unclear. A proper Ekman layer with the non-slip condition, as pointed out by one of the referees, may provide the adjustment across the Ekman boundary layer without substantially affecting the structure of interior convective flow. This is perhaps the most important issue of the problem which will be addressed in the future.

This work is supported by the SERC grant GR/H55437 and was written when I was at Isaac Newton Institute for Mathematical Sciences, Cambridge, 1992. I would like to thank an anonymous reviewer for his constructive comments.

REFERENCES

ALDRIDGE, K. D. 1972 Axisymmetric oscillations of a fluid in a rotating spherical shell. *Mathematika* **19**, 163–168.

ALDRIDGE, K. D. & LUMB, L. I. 1987 Inertial waves identified in the Earth's fluid outer core. *Nature* **325**, 421–423.

ALDRIDGE, K. D. & TOOMRE, A. 1969 Axisymmetric inertial oscillations of a fluid in a rotating spherical container. *J. Fluid Mech.* **37**, 307–323.

BUSSE, F. H. 1970 Thermal instabilities in rapidly rotating systems. *J. Fluid Mech.* **44**, 441–460.

BUSSE, F. H. 1982 Thermal convection in rotating systems. *Proc. 9th US Natl Congr. Appl. Mech.*, pp. 299–305. ASME.

BRYAN, G. H. 1889 The waves on a rotating liquid spheroid of finite ellipticity. *Phil. Trans. R. Soc. Lond.* A **180**, 187–219.

CARRIGAN, C. R. & BUSSE, F. H. 1983 An experimental and theoretical investigation of the onset of convection in rotating spherical shells. *J. Fluid Mech.* **126**, 287–305.

CHANDRASEKHAR, S. 1961 *Hydrodynamic and Hydromagnetic Stability*. Clarendon.

FEARN, D. R., ROBERTS, P. H. & SOWARD, A. M. 1988 Convection, stability and the dynamo. In *Energy, Stability and Convection* (ed. B. Straughan & P. Galdi), pp. 60–324. Longman.

GREENSPAN, H. P. 1968 *The Theory of Rotating Fluids*. Cambridge University Press.

LYTTLETON, R. A. 1953 *The Stability of Rotating Liquid Masses*. Cambridge University Press.

PROCTOR, M. R. E. 1994 Magnetoconvection in a rapidly rotating sphere. In *Stellar and Planetary Dynamos* (ed. M. R. E. Proctor & A. D. Gilbert). Cambridge University Press.

ROBERTS, P. H. 1968 On the thermal instability of a self-gravitating fluid sphere containing heat sources. *Phil. Trans. R. Soc. Lond.* A **263**, 93–117.

SOWARD, A. M. 1977 On the finite amplitude thermal instability of a rapidly rotating fluid sphere. *Geophys. Astrophys. Fluid Dyn.* **9**, 19–74.

ZHANG, K. 1991 Convection in a rapidly rotating spherical fluid shell at infinite Prandtl number: steadily drifting rolls. *Phys. Earth Planet. Inter.* **68**, 156–169.

ZHANG, K. 1992 Spiralling columnar convection in rapidly rotating spherical fluid shells. *J. Fluid Mech.* **236**, 535–556.

ZHANG, K. 1993 On equatorially trapped boundary inertial waves. *J. Fluid Mech.* **248**, 203–217.

ZHANG, K. & BUSSE, F. 1987 On the onset of convection in rotating spherical shells. *Geophys. Astrophys. Fluid Dyn.* **39**, 119–147.